This is a preprint, the final version is subject to change, of the American Mineralogist (MSA)
Cite as Authors (Year) Title. American Mineralogist, in press.
(DOI will not work until issue is live.) DOI: http://dx.doi.org/10.2138/am-2017-6117

Revision 2

Microscopic strain in a grossular-pyrope solution ***anti***correlates with excess volume through local Mg-Ca cation arrangement, more strongly at high Ca/Mg ratio

WEI DU[1,2], DAVID WALKER[2], SIMON MARTIN CLARK[3,4], XUEFEI LI[5], AND BAOSHENG LI[6]

[1] School of Earth and Space Sciences, Peking University, Beijing100871, China

[2] Lamont-Doherty Earth Observatory, Columbia University in the City of New York, Palisades, New York 10964, USA

[3]Department of Earth and Planetary Sciences, Macquarie University, North Ryde, NSW 2109, Australia

[4]The Bragg Institute, Australian Nuclear Science and Technology Organization, Locked Bag 2001, Kirrawee DC, NSW 2232, Australia

[5]Key Laboratory of Functional Materials Physics and Chemistry of the Ministry of Education, Jilin Normal University, Siping 136000, China

[6] Mineral Physics Institute, Department of Geosciences, Stony Brook University, Stony Brook, New York, 11794, USA

ABSTRACT

Unit cell volume and microstrain of $Py_{40}Gr_{60}$ garnets vary with synthesis temperature and annealing time, showing a strong **negative** correlation, as is also seen in another garnet solid solution, $Py_{20}Gr_{80}$. This anticorrelation is explained by local Ca-Mg cation arrangement in which Ca-Ca and Mg-Mg 3rd-nearest-neighbor (Same 3NN = S3NN) pairs form at rates other than those expected from random Ca-Mg distribution. S3NN pairs cause microstrain (Bosenick et al. 2000) but allow more efficient packing than random Ca-Mg pairings that contribute to excess volume, hence smaller cell volumes correlate with more microstrain. Both longer annealing time and higher heating temperature cause more S3NN formation, larger microscopic strain and smaller unit cell volume. The anticorrelation of microstrain and excess volume is weaker in our previous

study of pyrope-rich solutions (i.e., $Py_{80}Gr_{20}$, Du et al. 2016) because excess volume varies little from Ca-Ca S3NN pairings in pyrope-rich solutions, whereas Mg-Mg S3NN pairings in grossular-rich solutions studied here are effective at reducing excess volume. Heating to 600 °C under room pressure or cold hydrostatic compression to 10 GPa does not reset microstrain.

Margules' formulations for microstrain and volume as a function of Ca/Mg ratio captures these features, especially the two-peaked distribution of microstrain with composition discovered by Du et al. (2016). The similar two-peaked distributions of microstrain and excess energies derived from ab initio calculation with short range ordering of Mg and Ca cations (Vinograd and Sluiter 2006) indicate that the macroscopic thermodynamic mixing properties of solid solutions are directly related to arrangement of cations with large size misfit. The observed changes of microstrain with annealing temperature suggest that mixing properties measured from our pyrope-grossular garnet solid solutions synthesized at same temperature can serve as better experimental constrains for computational work.

Key words: pyrope-grossular garnet solid solution, high temperature, FWHM, microstrain, unit cell volume

INTRODUCTION

The garnet binary pyrope-grossular ($Mg_3Al_2Si_3O_{12}$-$Ca_3Al_2Si_3O_{12}$) provides an iconic solid-solution system for the study of non-ideal mixing behavior, because of the large size difference between divalent Mg^{2+} and Ca^{2+} (0.89 vs 1.12 Å in 8 coordination) (Shannon 1976). Enthalpy (Newton et al. 1977), low-temperature heat capacity (Haselton and Westrum 1980; Dachs and Geiger 2006), and volume (Ganguly et al. 1993; Bosenick and Geiger 1997; Bosenick et al. 2001; Du et al. 2016) all show positive deviations from idea mixing, whereas both volume derivatives, thermal expansion and bulk modulus, show negative deviation from ideal mixing (Du et al.

2015). Lattice strain arising from local structural heterogeneities in substitutional pyrope-grossular solid solutions has been thought to produce elastic energies that strongly affect the macroscopic enthalpy and volume of mixing (e.g., Geiger 2001, 2008; Dapiaggi et al. 2005). However, a more recent study by Du et al. (2016) shows that microstrain does not correlate well with either the positive excess mixing volume or enthalpy. Garnet solid solutions with composition $Py_{40}Gr_{60}$ show the largest positive deviation from ideal mixing volume, but carry almost no microstrain, unlike the large microstrains of garnets with compositions $Py_{80}Gr_{20}$ and $Py_{20}Gr_{80}$. In contrast, there appears to be a good anti-correlation between microstrain along pyrope-grossular garnet and their thermal expansions (e.g., see Figure 7 in Du et al. 2016), therefore, more work is needed to understand the effect of temperature on the microscopic strain and the puzzling anticorrelation between microstrain and unit cell volume.

The pyrope-grossular garnet structure has the space group $Ia\bar{3}d$, which contains SiO_4 tetrahedra and AlO_6 octahedra that are connected through corners and edges, building a three-dimensional quasi-framework with the divalent cations (Mg^{2+} and Ca^{2+}) located in the dodecahedral cavities. When the divalent cations (Mg^{2+} and Ca^{2+}) replace one another, the local structure will be modified and structural heterogeneities may be produced. The structural distortion around the "foreign" atom gives rise to strain energy. The total elastic strain in the pyrope-grossular solid solution thus depends on the ratio of Mg and Ca cations and the distribution of these two different divalent cations. Du et al. (2016) proposed that $Py_{40}Gr_{60}$ garnet, which has the smallest microstrain and the largest excess volume among the Ca-Mg compositions studied, has a larger degree of short range ordering of Mg and Ca cations. Ordering is used in the sense of Bosenick et al. (2000), taken as the avoidance of same cation Mg-Mg or Ca-Ca pairs as the third nearest neighbors (S3NN) in the dodecahedral sites during substitution

(Figure 1). $Py_{40}Gr_{60}$ with Mg:Ca ratio close to 1:1 has less possibility of randomly generated Mg-Mg or Ca-Ca 3NN pairings, thus shows an intrinsic degree of short-range ordering (e.g., Bosenick et al. 1995, 2000, 2001; Dove et al. 2000; Vinograd et al. 2004; Lavrentiev et al. 2006; Vinograd and Sluiter 2006). This less "strained" structure may have relatively large excess volume because Ca-Mg pairs pack less efficiently than strain-causing Mg-Mg and Ca-Ca S3NN pairs. The short range ordering of Mg/Ca in pyrope-grossular garnet was reported to decrease with increasing synthesis temperature (Bosenick et al. 1999). Thus, garnets synthesized at higher temperatures might be expected to exhibit larger microstrain as more strain-causing S3NN pairs are allowed. Therefore, the anticorrelation between microstrain and the short range ordering of Mg/Ca will be further supported if larger microstrain can be observed in garnets synthesized at higher temperatures. Thus, temperature would not relieve microstrain but would enhance it as a consequence of the anti-intuitive sort of disorder proposed and developed by Bosenick et al. (2000): the allowance of low-volume, strain causing S3NN pairs in proportion to composition alone.

The aim of the present study is to test the effect of temperature and/or annealing time on microstrain and excess volume, to explore whether there is a connection between microstrain and the arrangement of cations Ca and Mg. We chose $Py_{40}Gr_{60}$ glass as starting material because garnet crystals with this composition show the largest deviation from ideal mixing and almost no microstrain when synthesized at 6 GPa and 1400 °C. We synthesized garnet crystals of $Py_{40}Gr_{60}$ at 6 GPa within the range 1100-1700 °C with different annealing times (0.5 to 48 hours). Microstrain and unit cell volume of these garnet crystals were calculated from X-ray diffraction patterns collected with high resolution synchrotron light sources.

Different heating temperatures were also applied to another pyrope-poor garnet, $Py_{20}Gr_{80}$.

The result of a reheating experiment on $Py_{20}Gr_{80}$ is compared with a previously studied pyrope-rich composition $Py_{80}Gr_{20}$ (Du et al. 2016) in order to examine the possible difference in local environments of Mg and Ca inside garnet structures of variable composition and their effect on ordering status. We also examine the microstrains observed during thermal expansion determinations reported by Du et al. (2015) in reheating experiments (25 to 600 °C) at room pressure on garnet crystals quenched from 1400 °C and 6 GPa. The calculated microstrain value from these X-ray diffraction data was used to check whether reheating to modestly high temperature will change the microstrain and ordering status of cations. X-ray profiles at room temperature, high pressures were also collected to test whether cold elastic compression resets the microstrain of $Py_{40}Gr_{60}$.

EXPERIMENTAL METHODS

Synthesis of garnet crystals

Garnet solid solutions with two different compositions ($Py_{40}Gr_{60}$ and $Py_{20}Gr_{80}$) were synthesized from anhydrous glasses of stoichiometric composition. The same garnet glasses were also used in Du et al. (2015) and Du et al. (2016), which were prepared by melting a finely ground mixture of $CaCO_3$, MgO, Al_2O_3, and SiO_2 powders. The compositions of the glasses agree well with the starting proportion of oxides. More details about the preparation of garnet glasses can be found in Du et al. (2015).

The garnet crystals studied here were synthesized in a multi anvil (MA) device at the Lamont Doherty Earth Observatory (LDEO). In order to get pure garnet crystals, a Pt capsule was used to wrap the finely ground garnet glass, and this Pt capsule was then put into an Al_2O_3 tube before packing into the cylindrical cavity of a 3 mm inner diameter $LaCrO_3$ heater.

Crystalline garnets with composition ($Py_{40}Gr_{60}$) were synthesized at 6 GPa, but with different heating time at 1100, 1200, and 1400 °C. The synthesis or annealing conditions are summarized in Table 1. Garnet $Py_{40}Gr_{60}$ synthesized at 1400 °C/6 GPa/0.5 hour (experiment TT721, a = 11.722 ± 0.001 Å) was used as a standard to compare with those from various synthesis conditions. We tried to lengthen the quenching time in one synthesis experiment GG999 in order to test the assumption that ordering of Ca-Mg and loss of excess volume happened during quenching. After heating garnet glass ($Py_{40}Gr_{60}$) in MA device at 1400 °C for 0.5 hour, we set up a program to cool it from 1400 to 1100 °C in 15 minutes, much slower than the quenching time in experiment TT721, which was quenched by switching off powder after heating at 1400 °C for 0.5 hour, taking only a few seconds to drop temperature from 1400 to ~100 °C after crystallization and initial annealing at 1400 °C. Lower heating temperatures from 1000 to 1200 °C with heating time varied from 2 to 48 hours were applied to $Py_{40}Gr_{60}$ garnet glass (GG1001, GG1002, GG1003, GG1004, BB1007, and GG1005) to check the effect of synthesis temperature on microstrain. At relatively lower temperature (1100 and 1200 °C), longer annealing time as long as 24 hours is necessary to produce single phase homogeneous garnet. Garnet synthesized at 1400 °C for 0.5 hours heating was then put back in MA device and annealed for much longer time (GG1006) to check effect of the annealing time (48 hours) on microstrain and unit cell volume.

Garnet solid solution $Py_{20}Gr_{80}$ was synthesized (TT889) using the same batch of glass that was used to synthesize pure garnet at 6 GPa and 1400 °C (Du et al. 2016). Garnet glass was heated at 1300 °C and 6 GPa for only 5 minutes and then quenched to room temperature and pressure. The garnet crystal recovered from this short time synthesis experiment was embedded within KBr powder and put back into the MA device and pressured to 6 GPa and held at 1400 °C

for 100 minutes, and then quenched to room temperature (TT895) (Figure 2). The use of KBr pressure media was intended to limit mechanical damage to the crystal during recompression and reheating and thereby limit mechanical contributions to any observed microstrains. The KBr strategy to limit mechanical strain introduction was also used on $Py_{40}Gr_{60}$ with the GG1005 and BB1007 pair of experiments. [See caption to Figure 3.]

X-ray Diffraction

X-ray diffraction profiles for these $Py_{40}Gr_{60}$ garnets were collected at the Brookhaven National Lab (BNL) on beamline X17C in angular dispersive mode using an MAR345® image plate detector. The diffraction patterns were collected from 5° to 25° in 2θ angle with λ = 0.40722 Å (converted from energy ~30 keV) and the distance between sample and detector (~290 mm) was determined through collection of a standard LaB_6 diffraction pattern. X-ray diffraction patterns at high pressure up to 10 GPa were also collected for garnet product $Py_{40}Gr_{60}$ from experiment GG999. A four-screw symmetric diamond anvil cell was used for these measurements. More details about the data collection at high pressures can be found in Du et al. (2017).

Unit cell parameter of garnets $Py_{20}Gr_{80}$ were measured with X-ray diffraction at Advanced Light Source at Lawrence Berkeley National Lab (ALS) on station 12.2.2 at room temperature and pressure, in angular dispersive mode with MAR345® image plates as detectors. Garnet chunks were loaded in the ~120 μm diameter hole of a 60 μm thick steel gasket with the thrust axis perpendicular to the incident X-ray beam. The steel gasket was flipped over for the second measurement after the first X-ray reflection pattern was collected. The two measurements show perfect consistency with each other. The diffraction images were obtained with λ = 0.48593 Å converted from energy ~25 keV, and the distance between sample and the detector was

169 determined for each run to be ~440 mm through collection of a standard LaB_6 diffraction pattern.
170 The X-ray diffraction patterns were collected from 5° to 30° in 2θ.

171 FIT2D software package was used to integrate the two dimensional diffraction rings into
172 one-dimensional diffraction patterns (Hammersley et al. 1996). XFIT (Cheary and Coelho 1996)
173 and REFCEL (Cockcroft and Barnes 1997) were used to perform profile fitting analysis, which
174 determines the unit cell parameters from least squares analysis of the positions of the X-ray
175 diffraction peaks.

176 ## DATA ANALYSIS AND RESULTS

177 ### (1) Unit cell volume

178 The unit cell volumes of $Py_{40}Gr_{60}$ garnets synthesized at different temperatures with
179 different heating time are summarized in Table 1 and Figure 3a. The refined unit cell parameter
180 of $Py_{40}Gr_{60}$ from slow quenching experiment GG999 is 11.731 ± 0.001 Å, which is larger than
181 that from rapidly quenched experiment TT721 (a = 11.721 ± 0.001 Å). Garnet crystallized from
182 the same glass after heating at 1100 °C for 48 hours (GG1004) shows a similarly large unit cell
183 parameter (a = 11.732 ± 0.001 Å) as GG999, indicating that the relatively lower annealing
184 temperature (1100 °C) could be the principle reason for the larger unit cell volume. The unit cell
185 parameter of the garnet crystals measured at room temperature is an indication of the temperature
186 from which it has quenched suddenly, rather than the cooling rate of the sample to that
187 quenching temperature. The experiment BB1007 was carried at the same P-T-t condition as
188 GG1005 (1200 °C for 48 hours), and the unit cell parameter of garnet from BB1007 agrees well
189 with experiment GG1005, indicating the reproducibility of the current synthesis experiments.
190 The use of KBr in one experiment to limit mechanical strains, and not the other experiment, yet
191 achieving the same result, further suggests that mechanical strains are not contributing to the

192 microstrain. Garnet synthesized at 1200 °C shows smaller unit cell parameter (a = 11.725 ±
193 0.001 Å) than those heated at 1100°C (a = 11.732 ± 0.001 Å), indicating that garnets $Py_{40}Gr_{60}$
194 synthesized at higher temperatures show smaller unit cell volume. XRD measurement result of
195 $Py_{40}Gr_{60}$ garnet from experiment GG1000 gives a unit cell parameter a = 11.705 ± 0.001 Å,
196 much smaller than the "standard value" 11.722 Å (TT721). The reason for the termination of this
197 longer time annealing experiment is that temperature control failed and experimental temperature
198 shot too high during the long-term heating (Table 1). Such loss of temperature control to the high
199 side was proved by the melting of the Pt capsule used to isolate garnet glass from potential
200 contamination by $LaCrO_3$ heater. Melting temperature of Pt at 6 GPa is about 1950 °C, so we
201 believe there was a temperature excursion to as high as 1950 °C. The corresponding points for
202 this experiment in Figure 3 are plotted at 1700 °C with a right-directed horizontal arrow to
203 indicate that this is probably a minimum. Although we don't know the exact temperature of
204 experiment GG1000, it still implies that garnet that was heated at higher temperature has a
205 smaller unit cell volume.

206 However, experiment GG1006 ($Py_{40}Gr_{60}$), which reheated garnet crystals from experiment
207 TT721 (a = 11.722 ± 0.001 Å) as starting material, at 1400 °C and 6 GPa for much longer time
208 (48 hours) showed relatively smaller unit cell parameter (a = 11.715 ± 0.001 Å). We did the
209 same test on garnet $Py_{20}Gr_{80}$, results of which are presented in Table 2. The longer annealing
210 experiment TT895 ($Py_{20}Gr_{80}$) used product of experiment TT889 (1300 °C for 5 minutes) as
211 starting material and heated at higher temperature 1400 °C for longer time (100 minutes). And
212 we observed a slight shrinking of unit cell parameter from 11.807 ± 0.001 Å to 11.789 ± 0.001 Å
213 after second round annealing, showing consistent unit cell parameter as another experiment at
214 1400 °C (TT649). Therefore, longer annealing time at 1400 °C also reduces the unit cell volume

215 slightly. Figure 3a demonstrates that there is a systematic decrease in cell volume with synthesis
216 temperature of samples that are sufficiently annealed. At 1400 °C, a 0.5 hour anneal is not
217 sufficient to reach the systematic trend and the descending arrow shows the evolution of cell
218 parameter with increasing annealing time at 1400 °C to the systematic trend. The experiment
219 GG1000 listed as a minimum of 1700 °C reached the trend in a few seconds. As expected, the
220 required annealing time must be strongly temperature sensitive.

221

222 **(2) Microstrain**

223 The method described in Du et al. (2016) was used to calculate microstrain from the XRD
224 peaking broadening parameter η. The FWHM (full-width at half maximum) of LaB_6, which
225 does not change with 2θ angle up to 30º, was adopted as the instrumental broadening for
226 synchrotron XRD file, $B_{inst} \sim B_{LaB6}$. The XRD peak broadening of garnet sample, B_{garnet}, is
227 then determined by equation (1):

228 $$B_{garnet} \approx \sqrt{{B_{obs}}^2 - {B_{inst}}^2} \approx B_{obs} - B_{LaB_6} \qquad (1)$$

229 where B_{obs} is the FWHM of X-ray diffraction peaks fitted with pseudo-Voigt equations
230 (Langford 1978). The microstrain that contributes to the XRD peak broadening was calculated
231 through Williamson-Hall plots (Williamson and Hall 1953):

232 $$B_{garnet}\cos\theta = \frac{K\lambda}{<L>\cos\theta}\cos\theta + 4\eta\tan\theta\cos\theta = \frac{K\lambda}{<L>} + 4\eta\sin\theta \quad (2)$$

233 where λ is the wavelength of the X-ray, and θ is the Bragg angle (in radians), K is a constant of
234 value approximately 0.9 (Langford and Wilson 1978), L is the crystal size (diffraction domain

size), $\frac{K\lambda}{<L>\cos\theta}$ is the size effect on XRD peak broadening (Scherrer 1918), $4\eta\tan\theta$ is the width of the peak due to microstrain (Stokes and Wilson 1944), and η is the microstrain.

In order to minimize any systematic errors caused by different X-ray sources and to use the same LaB_6 pattern as instrumental contribution on XRD peak broadening, it is essential that all the XRD patterns were collected under the same instrumental condition. Therefore, we collected X-ray diffraction data on the same sample TT721 that was studied in Du et al. (2016) as reference. The microstrain data of garnets $Py_{40}Gr_{60}$ and $Py_{20}Gr_{80}$ were summarized in Table 1 and Table 2. For $Py_{40}Gr_{60}$ garnets with the same annealing time 48 hours (GG1004, GG1005, and GG1006), higher temperature 1400 °C caused more microstrain inside garnet structure (Figure 3), which is consistent with the reheating experiment on $Py_{80}Gr_{20}$ (Du et al. 2016), indicating that higher temperature annealing causes larger microstrain. Reheating experiments on $Py_{40}Gr_{60}$ show similar trends: that garnet annealed at higher temperature (> 1700 °C, GG1000) shows larger microstrain than that annealed at relatively lower temperature (1100 °C, GG999) (Figure 4). Reheating experiment on $Py_{40}Gr_{60}$ (GG1006), which used garnet crystals from experiment TT721 as starting material, at 1400 °C and 6 GPa for much longer time (48 hours) showed relatively larger microstrain 0.048% than that of TT721 (0.038%). Therefore, longer annealing time at 1400 °C also increases the microstrain slightly. Figure 3b shows a systematic relation increasing microstrain with temperature for sufficiently annealed samples, analogous to the cell size relation, but with opposite slope with temperature.

(3) Thermal expansion

X-ray diffraction patterns that were collected at room pressure to 600 °C by Du et al. (2015) from pyrope-grossular solid solutions powders were analyzed here by Williamson-Hall plots to

get the microstrain data at high temperatures. The results are present in Figure 5. Upon increasing temperature to 600 °C, the microstrain value of each garnet solid solution does not change with temperature. Evidently the microstrain does not reset with modest reheating. The two-peaked compositional dependence of microstrain along the pyrope-grossular garnet binary reported by Du et al. (2016) is demonstrated to hold at least up to 600 °C. There remain two distinct peaks in the microstrains of thermally expanded garnets, one at about $Py_{80}Gr_{20}$ and the other near $Py_{20}Gr_{80}$.

(4) Bulk modulus

In order to look for any effect of microstrain on compressional elastic properties, Birch-Murnaghan equation of state analysis was applied to the V-P data obtained for the specimen from experiment GG999 with the smallest observed microstrain (Table 3 and Figure 6). In the case of isothermal (room temperature) hydrostatic compression, the pressure can be written as:

$$P_V = 3K_0 f(1+2f)^{\frac{5}{2}}\left(1+\frac{3}{2}(K_0'-4)f\right) \qquad (3)$$

where f is the Eulerian finite strain (with sign reversed so f is positive for compression), $f = \frac{1}{2}\left[\left(\frac{V_P}{V_0}\right)^{-\frac{2}{3}} - 1\right]$, V_0 is the unit cell volume at ambient condition, K_0 is the isothermal bulk modulus at zero pressure, and K_0' is the first derivative of K_0 versus pressure. As discussed in Du et al. (2016), there is no constraint on K_0' of garnet with intermediate composition along pyrope-grossular garnet binary. Therefore, we tried fixed K_0' as 4.4 (Zhang et al. 1998) and 5.92 (Pavese et al. 2001), and calculated K_0 for $Py_{40}Gr_{60}$ by fitting the measured P-V data (Table 4 and Figure 6) to the Birch-Murnaghan (BM) Equation of State. For K_0' = 5.92, K_0 = 153.5 ± 1.0 GPa; similarly, K_0 = 158.6 ± 1.1 GPa for fixed K_0' = 4.4. Figure 7 shows the "normalized pressure" f_E

($f_E = P/(3f(2f+1)^{5/2})$ versus the volume Eulerian finite strain f plot (Angel 2000). The weighted linear regression through the data points yields the intercept value, $f_E(0)$ = 154.7 ± 1.0 GPa, which agrees with the result yielded from Birch-Murnaghan Equation of State. Thus, fitting these data to the third-order Birch-Murnaghan EoS yields a marginally smaller bulk modulus for GG999 compared with TT721 of 159.3 ± 1.0 GPa (average from Du et al. 2015). This lower value for GG999 is consistent with the general thought that crystals with larger excess volume are more compressible, showing a lower value for the bulk modulus.

In order to look for any effect of cold elastic compression on microstrain, values for microstrain at stages in the cold compression of GG999 are recorded in Table 3. There is no clear trend to increasing or decreasing microstrain with compression. It should be noted that the uncertainty in the microstrains reported in Table 3 are considerably greater than those reported in Tables 1 and 2 because of the fewer number of peaks collected at a more restricted range of 2θ imposed by the diamond anvil pressure cell. There is no resolvable effect of cold compression to 10 GPa on $Py_{40}Gr_{60}$ microstrain.

DISCUSSION

The substitution of Ca or Mg as "foreign" cations in pyrope or grossular garnets produces local distortions in the host structure because of the large size difference between Mg and Ca cations (Newton and Wood 1980; Bosenick et al. 2000). The importance of S3NN pairing for creating strains was demonstrated by Bosenick et al. (2000), but it was not clear from their lattice energy calculations that a two-peaked distribution of strain with garnet composition could result. Indeed, Dapiaggi et al. (2005) reported a single, asymmetric peak in strain for pyrope-grossular garnets synthesized with hydrothermal assistance. By contrast, Du et al. (2016) observed a two-peaked distribution with composition of microstrain in dry garnets all made at 1400 °C, 6 GPa,

303 in 0.5 hour that could be explained by the local arrangement of Mg/Ca. Our high resolution
304 synchrotron X-ray diffraction studies on newly synthesized garnets $Py_{40}Gr_{60}$ in this study further
305 show that both microstrain and unit cell volume change with synthesis and annealing
306 temperature and time. The relationship between unit cell volume and microstrain is a strong
307 anticorrelation for grossular-rich garnet solid solution (Figure 8). Higher heating temperature is
308 observed to produce smaller unit cell volumes. Lower synthesis temperature is consistent with
309 the relatively smaller microstrain in GG1004, which has a larger unit cell volume. Comparing the
310 specimens annealed for 48 hours, those annealed at higher temperature show larger microstrain
311 and relatively smaller unit cell volume (Table 2 and Figure 8). For experiments that use garnet
312 $Py_{40}Gr_{60}$ that was synthesized at 1400 °C and annealed for 0.5 hours as starting material, longer
313 time annealing at 1400 °C (GG1006) caused larger microstrain. And longer quenching time to
314 lower temperature (1100 °C) (GG999) partially releases microstrain (Figure 8). If as Du et al.
315 (2016) proposed, the microstrain data is correlated with the divalent cation (Mg and Ca)
316 arrangement in the pyrope-grossular garnet solid solutions, the result that we present in this study
317 implies that the longer annealing time and/or higher temperature processing causes larger
318 microstrain by forming the less energetic favored Mg-Mg and Ca-Ca pairs in garnet structures
319 (Bosenick et al. 2000). The smaller unit cell volumes observed for the more strained structures
320 are a consequence of Mg-Mg and Ca-Ca S3NN pairs packing more efficiently than Ca-Mg 3NN
321 pairs. Thus the microstrain – volume anticorrelation,

322 However, we observed systematically weaker anticorrelation between microstrain and unit
323 cell volume as garnet solutions become more pyrope-rich, unlike for grossular-rich garnets just
324 reported where the anticorrelation is strong. When garnets $Py_{80}Gr_{20}$ (TT890) and $Py_{20}Gr_{80}$
325 (TT889), that were both synthesized at 1300 °C, were later annealed at 1400 °C (TT895), each

326 gained more microstrain (Table 2 and Figures 8 and 9a). The $Py_{20}Gr_{80}$ (TT889 to TT895a) lost
327 volume as expected for grossular-rich garnets (Figure 9b). However, $Py_{80}Gr_{20}$, whose XRD
328 peaks also became broader after annealing at higher temperature 1400 °C, did so with less
329 significant changes in unit cell volume (Du et al. 2016). Therefore, the microstrain of S3NN Ca-
330 Ca pair formation changes the unit cell volume of pyrope-rich garnet ($Py_{80}Gr_{20}$) less than Mg-Mg
331 pairs reduce the unit cells of grossular-rich garnets. This observation could be explained by the
332 different local environment of Mg and Ca cations between garnets with composition close to the
333 two different end members pyrope and grossular as proposed by Oberti et al. (2006) and
334 Quartieri et al. (2008). The local environments around Ca and Mg cations inside pyrope-
335 grossular garnet are different for different compositions. Formation of Ca-Ca pairs in Mg-rich
336 environments has less impact on expanding the volume than Mg-Mg pairs' effect on lattice
337 collapse in Ca-rich environments.

338 This argument is foreshadowed by the 'forbidden region' argument Newton and Wood
339 (1980) used to explain S-shaped volume curves with negative excess volumes near the small-
340 end-membered end of a solid solution series and positive excesses near the larger end member.
341 Large cations in a small cation matrix are inserted with local lattice stretches that do not cause
342 global lattice expansion until the large cations interact. The local stretch creates an energetically
343 forbidden environment where another local large cation would be unfavorably sited. The
344 proposition in Newton and Wood (1980) was that such strains would be encountered between
345 S1NN pairs. Bosenick et al. (2000) showed that the S3NN pairs were a much more likely pairing
346 from a lattice energetics perspective to cause local strains. If one shifts perspective from S1NN
347 to S3NN pairs, the framing of the problem and arguments of Newton and Wood (1980) continue
348 to make physical sense and to form the basis of an avoidance model. This preferential avoidance

(a form of cation ordering) keeps the large cations from interacting globally over the whole lattice in such a way that lattice expansion is not as much as expected for the proportion of large cation substituents. Likewise, when small cations enter a large cation matrix, their ability to cause global lattice shrinkage is diminished, except for the fact that it is more difficult to resist a collapse against no sustaining outward force than to resist a stretch against strong constraining forces. Thus the negative deviations from ideality at the small end-member are expected to be greater than the positive deviations at the large end member of the series. Newton and Wood (1980) showed a number of mineralogical solutions that give examples of this behavior. The application to our garnets is that the S3NN pairs behave differently when it is Mg-Mg in a grossular-rich matrix compared to Ca-Ca in a pyrope-rich matrix. By the Newton and Wood (1980) arguments we expect volume variations driven by cation avoidances to be more suppressed at the small-end-member pyrope-rich end of the series.

Do microstrain and related excess volume changes cause significant changes in minerals' physical properties, for example, elastic moduli (Hazen and Navrotsky 1996)? The unit cell volume of $Py_{40}Gr_{60}$ garnet GG999 shows compression similar to that from TT721 (Figure 6), although the former shows relatively smaller microstrain and larger unit cell volume. Fitting these data to the third-order Birch-Murnaghan EoS yields a marginally smaller bulk modulus (~154 GPa) for GG999 comparing with TT721 (~158 GPa) (Du et al. 2015). Considering the fact that the microstrain calculated from FWHM of X-ray pattern does not change with pressure up to 10 GPa (Du et al. 2016), which means that microstrain does not change during compression, the smaller bulk modulus of GG999 compared with that of TT721 may be related to the relatively larger unit cell volume. This suggestion is supported by the observation that garnet solid solutions with composition closer to the end members, for example $Py_{20}Gr_{80}$ and $Py_{80}Gr_{20}$

372 which show larger microstrain and relatively smaller excess volume, have larger bulk moduli
373 (Du et al. 2015). Our new data for $Py_{40}Gr_{60}$ is consistent with previous study that pyrope-
374 grossular garnet solid solution with composition close to 50:50 shows smaller bulk modulus, thus
375 larger compressibility than the two end members. However, as mentioned above, the parameters
376 K_0 and K_0' are usually strongly correlated in equation of state fitting (e.g. Nishihara et al. 2003),
377 and the substitution between Ca and Mg in the dodecahedral X site may affect the K_0' (Conrad et
378 al. 1999) but cannot be resolved by the current data.

379 Why does increasing annealing time favor more strain? It is unsettling to have the
380 evolution with annealing time be to a state of higher microstrain. The usual expectation is that
381 annealing relieves strains. However, the microstrains observed in garnet are unusual in that they
382 provide better packing through the formation of S3NN pairs. Thus the volume reduction provides
383 the incentive at high pressure to increase strain. One might expect that higher temperature should
384 disorder a system and thus relieve strain. However, increasing the number of S3NN pairs is not
385 disordering, because it may also increase the departures from random Ca-Mg arrangement. Thus
386 the clear anticorrelation of V_{ex} and microstrain across all the temperatures studied to both higher
387 and lower values than the disordered glass starting material, suggests that an order/disorder
388 framework is not a productive perspective here. 'Ordering' increases towards both ends of the T-
389 V_{ex}-microstrain spectrum and cannot monotonically drive the evolution of properties we observe.

390 Given that we deduce that neither 'ordering' nor local lattice energetics is a completely
391 satisfactory explanation for our anticorrelation, or for the two-peaked distribution of microstrain
392 with composition, we attempt to describe the system as one in which Ca-Mg arrangements are
393 basically set by bulk composition, with minor strain perturbations that add asymmetry to the
394 response with composition. The Margules form of mixing properties has as its basis that

395 substitutional elements will interact in proportion to their probability of being paired based on
396 the composition of the mix. If the placement is random, then the symmetric form of Margules
397 mixing results. If the pairs form with unbalanced interaction parameters, then the asymmetric
398 form results. The strains in the garnet solution come from the misfits of Ca into an Mg matrix (or
399 Mg into a Ca matrix). Ca-Mg pairs intrinsically have excess volume compared to SNN pairs. We
400 can pass over the issue of whether we do the bookkeeping on S1NN or S3NN pairs as the
401 population probabilities are the same. The probability of forming Ca-Mg pairs in a mixed garnet
402 is $2X_{Py}X_{Gr}$. The probability is zero at either end member and ½ at the equimolar intermediate
403 composition. The remaining half is ¼ each of Mg-Mg and Ca-Ca pairs. The excess volume
404 strains should then maximize at the Ca-Mg pair maximum in the middle of the series. However,
405 the XRD microstrains respond to the formation of Ca-Ca strain-producing pairs in an Mg-Mg
406 matrix (and vice versa). The fraction of these pairs rise as $X_{Gr}X_{Gr}$ near pyrope (or $X_{Py}X_{Py}$ near
407 grossular). This increase in Ca-Ca microstrain is modified away from the end member pyrope by
408 the erosion of the matrix of Mg-Mg pairs at rate $X_{Py}X_{Py}$ through the formation of Ca-Mg and Ca-
409 Ca pairs that do not contribute to the XRD strain contrast between the Ca-Ca pairs and the Mg-
410 Mg matrix. [Effectively there is a discount rate for the growth of microstrain.] Thus the variation
411 of microstrain may be expected to go as the difference of the squares of X_{Py} and X_{Gr}. This form
412 of microstrain can lead to a two-peaked maximum in microstrain across the pyrope-grossular
413 series, unlike the Dapiaggi data or the Bosenick energetics.

414 We propose that the excess volumes with their volume strains form a basis for modeling
415 the form of microstrains strains that arise through Ca-Mg, Ca-Ca, or Mg-Mg pair misfits. When
416 asymmetry for unequal Mg-Mg vs. Ca-Ca interactions is allowed, the $X_{Py}X_{Gr}$ $(X_{Py}W_{\eta_{Gr}} + X_{Gr}W_{\eta_{Py}})$
417 form gives this basic driver for strain with Margules parameters $W_{\eta_{Py}}$ and $W_{\eta_{Gr}}$ reflecting the

418 possibly unequal excess strains associated with forming Ca substitutions into pyrope and Mg
419 substitutions into grossular. This is, of course, the same form of the Margules volume mixing
420 equation in which $V_{ex} = \mathrm{X_{Py}X_{Gr}}(\mathrm{X_{Py}}W_{V_{Gr}} + \mathrm{X_{Gr}}W_{V_{Py}})$, the W_V parameters giving the volume
421 interactions rather than the W_η for strain. The basic Margules form for strain must be discounted
422 as Ca-Mg random pairs begin to accumulate in the structure and disrupt the distortional and
423 torsional strains introduced by Ca-Ca and Mg-Mg S3NN pairings. [They do not disrupt the
424 accumulating volume strain of Ca-Mg misfit.] The strain disruption discount depends on the
425 difference between Ca-Ca and Mg-Mg pairings, for which we propose $\left(\left|\mathrm{X_{Gr}^2} - \mathrm{X_{Py}^2}\right| - W_0\right)$,
426 giving:

427 $$\text{Strain} = \eta = \mathrm{X_{Py}X_{Gr}}(\mathrm{X_{Py}}W_{\eta_{Gr}} + \mathrm{X_{Gr}}W_{\eta_{Py}})\left(\left|\mathrm{X_{Gr}^2} - \mathrm{X_{Py}^2}\right| - W_0\right) \quad (4)$$

428 W_o is an adjustable scaling parameter that allows the possibility that strain not go strictly to
429 zero when the number of Mg-Mg and Ca-Ca pairs are equal. Figure 10 shows the observed
430 microstrains fit to the Margules-inspired form given above. The Margules form captures the two-
431 peaked distribution of microstrain with composition in this solution series prepared at 6 GPa,
432 1400 °C. A small $W_0 = 0.07 \pm 0.02$ is indicated, although eliminating W_0 degrades the fit only
433 slightly. $W_{\eta_{Py}}$ (1.44 ± 0.36) and $W_{\eta_{Gr}}$ (1.19 ± 0.02) are comparable in magnitude and have a ratio
434 that is within a few percent of the inverse ratio of the cation radii (1.12/0.89). The W_η Margules
435 parameters for strain have an analogous physical meaning to the W_V parameters for excess
436 volume. If the tangent to the excess strain curve at $X_{Gr} = 1$ is extrapolated to $X_{Gr} = 0$ (i.e. to $X_{Py} =$
437 1), the intercept has the value $W_{\eta_{Py}}$. Likewise $W_{\eta_{Gr}}$ is the intercept at $X_{Gr} = 1$ of the extrapolated
438 tangent to the excess strain curve at $X_{Gr} = 0$. The one-peaked asymmetric volume strain pattern
439 seen in Figure 9b drives both volume and local distortional strain by Mg-Ca size misfit. This

440 driver competes with the strain-reducing disruption of a dropping population of Mg-Mg and Ca-
441 Ca pairs as bulk compositions approach 50:50, resulting in the strains being maximized in
442 separate domains of composition space near 20% of either end member.

443 This two-peaked strain pattern does not resemble that of Dapiaggi et al. (2005) measured
444 on garnets prepared differently with hydrothermal assistance. However, the data of Dapiaggi et
445 al. (2005) can also be fit with this fairly flexible form but would require grossly asymmetric
446 $W_{\eta_{Py}}$ and $W_{\eta_{Gr}}$ to accommodate the single peak towards pyrope-rich compositions. Such gross
447 asymmetry would contradict the prescription of Bosenick et al. (2000) that strain effects should
448 be symmetric. Symmetric does not preclude two peaks in strain, but this was not a conspicuous
449 conclusion of the Bosenick et al. (2000) study. Our Margules form can be compatible with the
450 Bosenick result with large negative W_0. These differences among theory and two experimental
451 studies are important to resolve to understand the controls on intracrystalline strains. The
452 experimental differences may reflect differences in garnet preparation techniques between these
453 studies, or differences in data reliability. We have reproduced our data on powder samples and
454 chunks with two synchrotrons and one lab source data collection platforms with acceptable
455 success, and at least the Margules model provides a rationale for understanding the two-peaked
456 strain distribution which is only seen by us.
457

458 **IMPLICATION**

459 Does the protocol for sample preparation make any difference to the understanding of
460 solution behavior in mineral solutions? The volume-microstrain relations of dry pyrope-grossular
461 garnets grown at 6 GPa by Du et al. (2016) are quite different from those reported by Dapiaggi et
462 al. (2005) grown with hydrothermal assist at lower pressures. Our strains anticorrelate with

463 excess volume and are bimodally peaked in composition. We have been able to reproduce our
464 bimodal strain-volume-composition relations on different sample sets on two different diffraction
465 platforms. The strains in hydrothermally assisted garnet solutions are not bimodal, and have a
466 variation with composition that mimics the excess enthalpy of solution of hydrothermally
467 assisted garnets of Newton et al. (1977). Our bimodal strains on dry garnets do not correlate with
468 the excess enthalpy of hydrothermally assisted garnets, but resemble the mixing entropy
469 calculated for different states of order of the Mg and Ca cations (Vinograd and Sluiter 2006). So
470 the implied answer to the question is yes.

471 Our new observation of the anticorrelation between microstrain and unit cell volume
472 indicates that the arrangement of cations with size misfit affects the thermodynamic mixing
473 properties of a solid solution and the degree of this effect changes with annealing temperature
474 and hydrothermal assistant. Garnet solid solutions that were synthesized at same pressure and
475 temperature conditions should serve as better experimental constrains for modern quantitative
476 computational work. Mixing properties of pyrope-grossular garnet solid solutions that were used
477 for geothermal barometers need more work to update.

478

479 **ACKNOWLEDGMENTS**

480 The authors thank Associate Editor Dr. Haozhe Liu and two anonymous reviewers for their
481 perceptive reviews. We thank Dr. Bernard J. Wood for his thoughtful review during preparation
482 of this work. This work was supported by the U.S. National Science Foundation. The Advanced
483 Light Source is supported by the Director, Office of Science, Office of Basic Energy Sciences, of
484 the U.S. Department of Energy under Contract No. DE-AC02-05CH11231 at Lawrence Berkeley
485 National Laboratory. This work was also supported by DOE/NNSA Grant No. DE-NA0001815
486 and NSF Grant No. EAR1045630 to B. Li. We thank Jean Hanley, Jinyuan Yan, and Zhiqiang
487 Chen for their technical assistance.

488

489

REFERENCES CITED

Angel, R.J. (2000) Equations of state. In: Hazen, R.M. and Downs, R.T., Editors, High-pressure and high-temperature crystal chemistry. Review in Mineralogy and Geochemistry, 41, 35–60.

Bosenick, A. and Geiger, C.A. (1997) Powder X-ray diffraction study of synthetic pyrope-grossular garnets between 20 and 295 K. Journal of Geophysical Research, 102, 22649–22657.

Bosenick, A., Dove, M.T., and Geiger, C.A. (2000) Simulation studies on the pyrope-grossular garnet solid solution. Physics and Chemistry of Minerals, 27, 398–418.

Bosenick, A., Dove, M.T., Heine, V., and Geiger, C.A. (2001) Scaling of thermodynamic mixing properties in garnet solid solutions. Physics and Chemistry of Minerals, 28, 177–187.

Bosenick, A., Geiger, C.A., Schaller, T., and Sebald, A. (1995) A ^{29}Si MAS NMR and IR spectroscopic investigation of synthetic pyrope-grossular garnet solid solutions. American Mineralogist, 80, 691–704.

Cheary, R.W. and Coelho, A.A. (1996) Programs XFIT and FOURYA, deposited in CCP14 powder diffraction library. Engineering and Physical Sciences Research Council, Daresbury Laboratory, Warrington, England.

Conrad, P.G., Zha, C.S., Mao, H.K., and Hemley, R.J. (1999) The high-pressure, single-crystal elasticity of pyrope, grossular, and andradite. American Mineralogist, 84, 374–383.

Dachs, E. and Geiger, C.A. (2006) Heat capacities and entropies of mixing of pyrope-grossular ($Mg_3Al_2Si_3O_{12}$-$Ca_3Al_2Si_3O_{12}$) garnet solid solutions: A low-temperature calorimetric and a thermodynamic investigation. American Mineralogist, 91, 894–906.

511 Dapiaggi, M., Geiger, C.A., and Artioli, G. (2005) Microscopic strain in synthetic pyrope-
512 grossular solid solutions determined by synchrotron X-ray powder diffraction at 5 K: The
513 relationship to enthalpy of mixing behavior. American Mineralogist, 90, 506–509.
514 Dove, M.T., Bosenick, A., Myers, E.R., Warren, M.C., and Redfer, S.A.T. (2000) Modeling in
515 relation to cation ordering. Phase Transitions, 71, 205–226.
516 Du, W., Clark, S.M., and Walker, D. (2015) Thermo-compression of pyrope-grossular garnet
517 solid solution: non-linear compositional dependence. American Mineralogist, 100, 215–222.
518 Du, W., Clark, S.M., and Walker, D. (2016) Excess mixing volume, microstrain, and stability of
519 pyrope-grossular garnets. American Mineralogist, 101, 193–204.
520 Du, W., Li, X., and Li, B. (2017) Microstrain in pyrope-grossular garnet solid solution at high
521 pressure: a case study of $Py_{90}Gr_{10}$ and $Py_{10}Gr_{90}$ up to 15 GPa. Physics and Chemistry of
522 Minerals, 44, 377–388.
523 Freeman, C.L., Allan, N.L., and van Westrenen, W. (2006) Local cation environments in the
524 pyrope-grossular $Mg_3Al_2Si_3O_{12}$-$Ca_3Al_2Si_3O_{12}$ garnet solid solution. Physical Review B, 74,
525 134203.
526 Ganguly, J., Cheng, W., and O'Neill, H.C. (1993) Syntheses, volume, and structural changes of
527 garnets in the pyrope-grossular join; implications for stability and mixing properties.
528 American Mineralogist, 78, 583–593.
529 Geiger, C.A. (2001) Thermodynamic mixing properties of binary oxide and silicate solid
530 solutions determined by direct measurements: The role of strain. In Geiger, C.A. Ed, Solid
531 Solutions in Silicate and Oxide Systems, 3, 71–100. European Notes in Mineralogy, Eötvös
532 University Press, Budapest.

Geiger, C.A. (2008) Silicate garnet: A micro to macroscopic (re)view. American Mineralogist, 93, 360–372.

Hammersley A.P., Svensson S.O., Hanfland M., Fitch A.N., and Häusermann D. (1996) Two-dimensional detector software: from real detector to idealized image or two-theta scan. High Pressure Research, 14, 235–248.

Haselton Jr., H.T. and Westrum Jr., E.F. (1980) Low-temperature heat capacities of synthetic pyrope, grossular, and $pyrope_{60}grossular_{40}$. Geochimica et Cosmochimica Acta, 44, 701–709.

Hazen, R.M. and Navrotsky, A. (1996) Effect of pressure on order-disorder reactions. American Mineralogist, 81, 1021–1035.

Langford, J.I. (1978) A rapid method for analyzing the breadths of diffraction and spectral lines using the Voigt function. Journal of Applied Crystallography, 11, 10–14.

Langford, J.I. and Wilson, A.J.C. (1978) Scherrer after sixty years: a survey and some new results in the determination of crystallite size. Journal of Applied Crystallography, 11, 102–113.

Lavrentiev, M.Y., van Westrenen, W., Allan, N.L., Freeman, C.L., and Purton, J.A. (2006) Simulation of thermodynamic mixing properties of garnet solid solutions at high temperatures and pressures. Chemical Geology, 225, 336–346.

Newton, R.C., Charlu, T.V., and Kleppa, O.J. (1977) Thermochemistry of high pressure garnets and clinopyroxenes in the system CaO-MgO-Al_2O_3-SiO_2. Geochimica et Cosmochimica Acta, 41, 369–377.

Newton, R.C. and Wood, B.J. (1980) Volume behavior of silicate solid solution. American Mineralogist, 65, 733–745.

555 Nishihara, Y., Takahashi, E., Matsukage, K.N., and Kikegawa, T. (2003) Thermal equation of
556 state of omphacite. American Mineralogist, 88, 80–86.
557 Oberti, R., Quartieri, S., Dalconi, M.C., Boscherini, F., Iezzi, G., Boiocchi, M., and Eeckhout,
558 S.G. (2006) Site preference and local geometry of Sc in garnets: Part I. Multifarious
559 mechanisms in the pyrope-grossular join. American Mineralogist, 91, 1230–1239.
560 Pavese, A., Levy, D., and Pischedda, V. (2001) Elastic properties of andradite and grossular, by
561 synchrotron X-ray diffraction at high pressure conditions. European Journal of Mineralogy,
562 13, 929–937.
563 Quartieri, S., Boscherini, F., Dalconi, C., Iezzi, G., Meneghini, C., and Oberti, R. (2008)
564 Magnesium *K*-edge EXAFS study of bond-length behavior in synthetic pyrope-grossular
565 garnet solid solutions. American Mineralogist, 93, 495–498.
566 Scherrer, P. (1918) Bestimmung der Grösse und der inneren Struktur von Kolloidteilchen mittels
567 Röntgenstrahlen. Nachrichten der Kgl Gesellschaft der Wissenschaftern zu Göttingen, 26,
568 98–100.
569 Shannon, R.D. (1976) Revised effective ionic radii and systematic studies of interatomic
570 distances in halides and chalcogenides. Acta Crystallographica A, 32, 751–767.
571 Stokes, A.R. and Wilson, A.C. (1944) The diffraction of X rays by distorted crystal aggregates.
572 Proceedings of the Physical Society, 56, 174–181.
573 Vinograd, V.L. and Sluiter, M.H.F. (2006) Thermodynamics of mixing in pyrope-grossular,
574 $Mg_3Al_2Si_3O_{12}$-$Ca_3Al_2Si_3O_{12}$, solid solution from lattice dynamics calculations and Monte
575 Carlo simulations. American Mineralogist, 91, 1815–1830.

576 Vinograd, V.L., Sluiter, M.H.F., Winkler, B., Putnis, A., Hålenius, J.D.G., and Becker, U. (2004)
577 Thermodynamics of mixing and ordering in pyrope-grossular solid solution. Mineralogical
578 Magazine, 68(1), 101–121.
579 Williamson, G.K. and Hall, W.H. (1953) X-ray broadening from filled aluminum and wolfram.
580 Acta Metallurgica, 1, 22–31.
581 Zhang, L., Ahsbahs, H., and Kutoglu, A. (1998) Hydrostatic compression and crystal structure of
582 pyrope to 33GPa. Physics and Chemistry of Minerals, 25, 301–307.
583

584 **TABLE 1.** Unit cell parameter and microstrain of garnet solid solution $Py_{40}Gr_{60}$ synthesized at 6
585 GPa and different temperatures with different annealing time, measured with synchrotron X-ray
586 diffraction at BNL

Experiment	Temperature (°C)	Heating time (hour)	Unit cell parameter (Å/cell)	Microstrain (%)	Remarks
TT721	1400	0.5	11.722(5)	0.038(10)	Garnet used in previous studies (Du et al. 2015, 2016)
GG999	1400	0.5	11.731(1)	0.022(3)	Heated at 1400 °C for 30 minutes and cooled slowly to 1100 °C
GG1000	*	*	11.705(1)	0.072(5)	Synthesized 1400 °C for 30 minutes and heated at 1200 °C for 1 day, *but ended with blow out; temperature may have been higher than 1700 °C briefly because the Pt capsule melted
GG1001	1200	24	11.725(1)	0.048(9)	Single phase garnet
GG1002	1000	48	n.a	n.a	Garnet with much broader peaks, possible two phases
GG1003	1100	2	n.a	n.a	Pyroxene coexists with garnets and glass
GG1004	1100	48	11.732(1)	0.031(8)	Single phase garnet
BB1007	1200	48	11.720(1)	0.045(3)	Start from big glass chunks in KBr and product is single phase garnet
GG1005	1200	48	11.721(1)	0.048(4)	Start from glass powder and product is single phase garnet
GG1006	1400	48	11.715(1)	0.059(3)	Starting material is product of TT721

587
588
589
590
591
592
593
594

TABLE 2. Unit cell parameter and microstrain of garnets $Py_{20}Gr_{80}$ and $Py_{80}Gr_{20}$ measured with synchrotron X-ray diffraction at ALS

	Experiment	Starting material	Temperature (°C)	Time (hour)	Unit cell parameter (Å)	Microstrain (%)
$Py_{20}Gr_{80}$	TT649	glass	1400	0.5	11.787(1)	0.099(4)
	TT889	glass	1300	0.1	11.807(1)	0.065(2)
	TT895a	Product of TT889	1400	1.6	11.789(1)	0.081(5)
$Py_{80}Gr_{20}$ (Du et al. 2016)	TT724	glass	1400	0.5	11.542(3)	0.101(3)
	TT890	glass	1300	0.1	11.543(2)	0.036(3)
	TT895b	Product of TT890	1400	1.6	11.540(2)	0.102(3)

TABLE 3. Unit cell parameter of garnet $Py_{40}Gr_{60}$ (GG999 with large excess volume and low microstrain) at different pressure measured with synchrotron X-ray diffraction at BNL

P(GPa)*	a(Å)	V(Å^3)	Microstrain (%)	f_E	F_E (GPa)
0	11.730(1)	1614.1(2)	0.032(5)	0.000(1)	0.000
0.9	11.709(1)	1605.4(4)	0.043(26)	0.002(1)	155.5±4.6
1.5	11.694(1)	1599.1(2)	0.012(11)	0.003(1)	156.1±2.5
2.7	11.665(1)	1587.3(5)	0.059(16)	0.006(1)	158.0±2.9
3.6	11.646(1)	1579.4(5)	0.006 (27)	0.007(1)	157.4±2.5
4.0	11.635(1)	1575.2(6)	0.003(21)	0.008(1)	156.0±2.1
4.6	11.624(1)	1570.7(5)	0.006(29)	0.009(1)	159.6±1.7
5.1	11.612(1)	1565.9(5)	0.052(33)	0.010(1)	157.7±1.9
5.5	11.603(1)	1562.2(6)	0.034(17)	0.011(1)	156.1±1.7
6.4	11.584(1)	1554.4(6)	0.100(30)	0.013(1)	156.3±1.9
7.0	11.576(2)	1551.3(7)	0.044(21)	0.013(2)	161.6±1.7
7.4	11.565(1)	1546.9(5)	0.049(21)	0.014(1)	160.6±2.0
8.5	11.544(2)	1538.6(7)	0.002(23)	0.016(2)	160.4±1.2
9.3	11.530(1)	1532.7(5)	0.094(27)	0.018(1)	162.2±1.0
10.3	11.510(1)	1524.9(5)	0.051(42)	0.019(1)	161.4±1.0

*the uncertainties of the pressure values constrained from the pressure measured before and after data collection are about 0.1-0.2 GPa

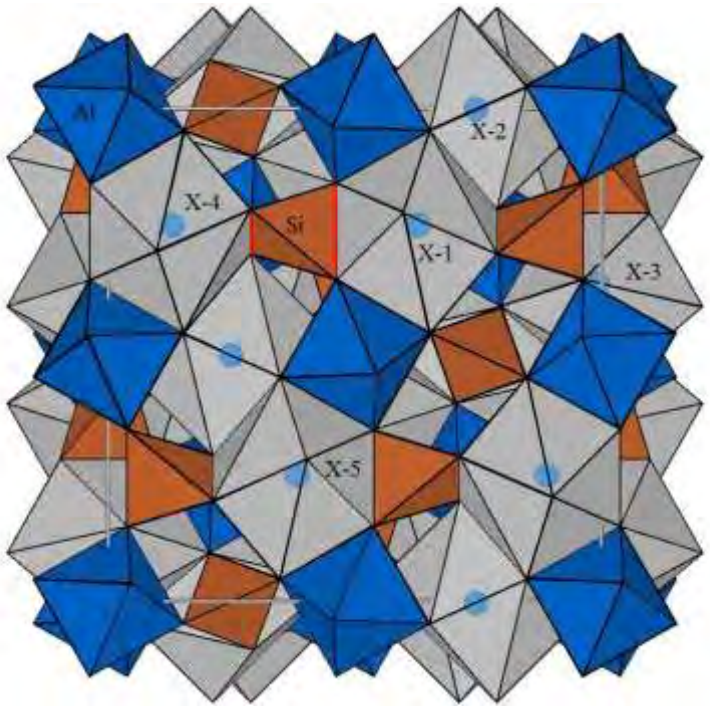

FIGURE 1. Polyhedral model of the pyrope-grossular garnet structure showing the dodecahedra (gray) and their linkage to the SiO_4 tetrahedra (orange) within one unit-cell. The nearest neighbors for two dodecahedra are (X-1) and (X-2). The second nearest neighbors are (X-1) and (X-3), one dodecahedron is edge shared with SiO_4 tetrahedron and another dodecahedron is corner shared with the same SiO_4 tetrahedron. The third nearest neighbor (3NN) dodecahedra are (X-1) and (X-4) that are both edge shared (the red lines) with the same SiO_4 tetrahedron. As suggested by Bosenick et al. (2000) the third nearest neighbor positions are the least energetically favored by Mg-Mg or Ca-Ca pairs because the double edge sharing of SiO_4 tetrahedron between X-1 and X-4 dodecahedra resists axial and torsional distortions imposed by strain.

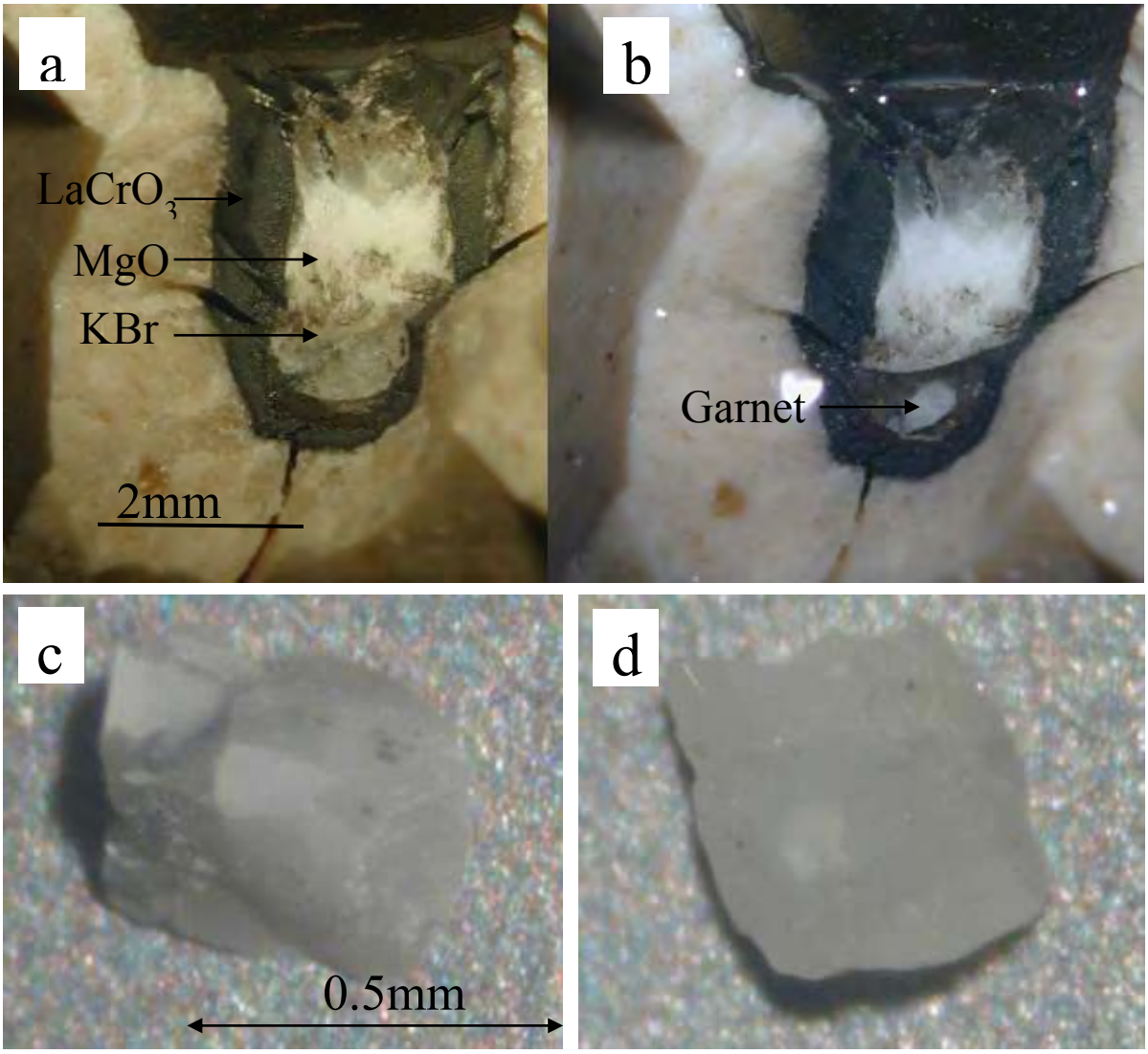

FIGURE 2. a Pictures showing the set-up of reheating experiment (TT895) on $Py_{20}Gr_{80}$, KBr powder was used to protect the garnet crystal from crushing at higher pressure; **b** After washing away KBr powder by distilled water, garnet crystal was recovered without damage; **c** Garnet crystal synthesized from glass at 1300 ºC and 6 GPa for only 5 minutes heating was used as starting material for further annealing experiment; **d** recovered garnet sample after annealing at higher temperature. Note that there is little difference in appearance before and after further annealing except for smoothing of the sharp edges and subduing of some cracks.

644

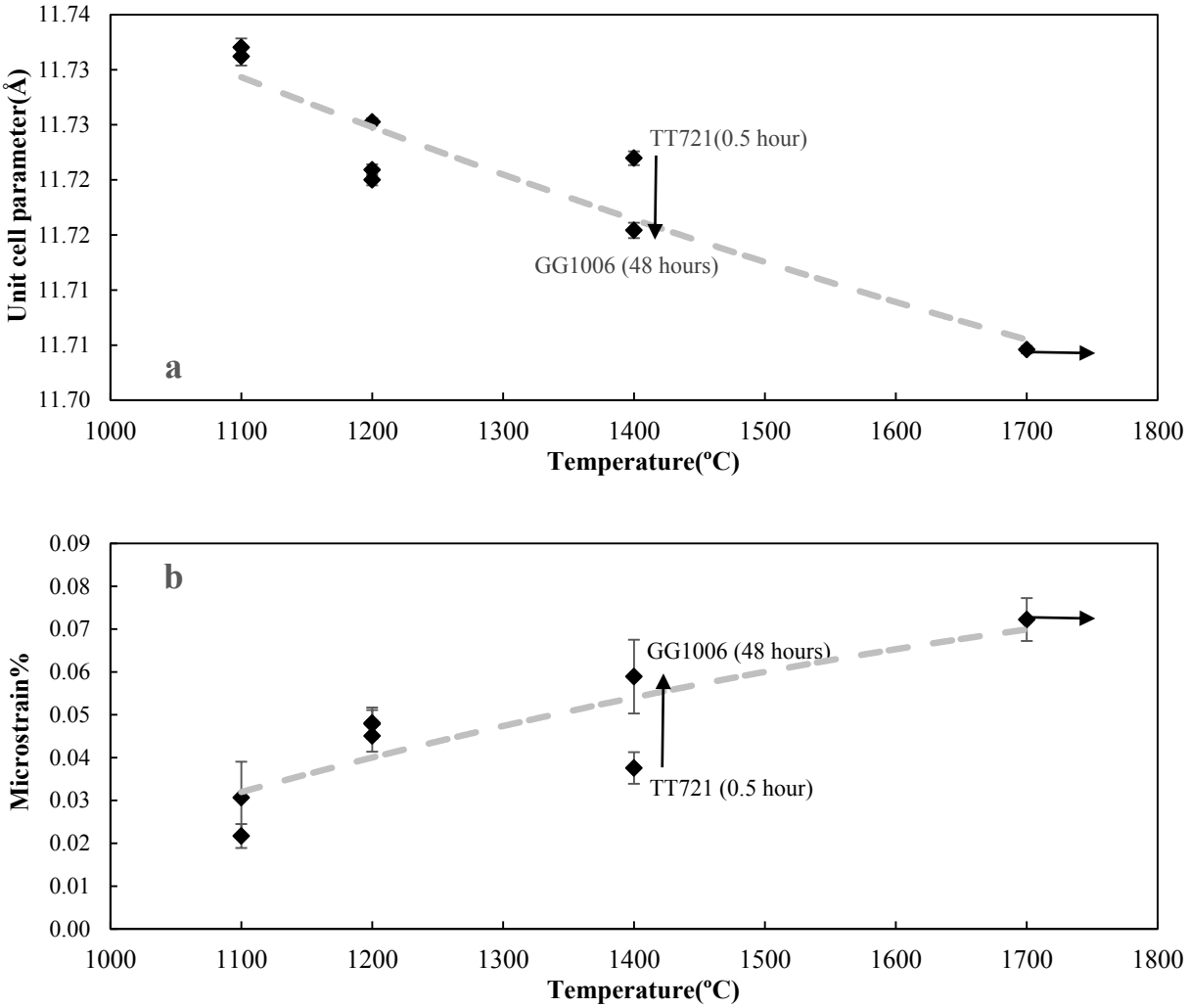

645

646

647 **FIGURE 3.** Cell parameters (**a**) and microstrains (**b**) of garnets ($Py_{40}Gr_{60}$) synthesized at
648 different temperatures and annealed for times up to 48 hours. Higher temperature annealing
649 causes more XRD peak broadening, and thus larger microstrain. Cell parameters decrease with
650 both annealing time and higher temperature in a systematic way for sufficient annealing times.
651 Microstrains grow with both annealing time (vertical arrows at 1400 °C) and higher temperature
652 (x axis). GG1005 and GG1007, both at 1200 °C, show very good reproducibility. They differ in
653 that GG1007 used a single chunk of glass starting material surrounded by KBr to prevent
654 mechanical damage during compression from adding to the microstrains of Ca-Mg
655 rearrangement. GG1005 was finely ground glass powder without such mechanical isolation from
656 shear strain during compression. The reproducibility of GG1005 and GG1007 suggest that
657 mechanical microstrains are not in play.

658

659

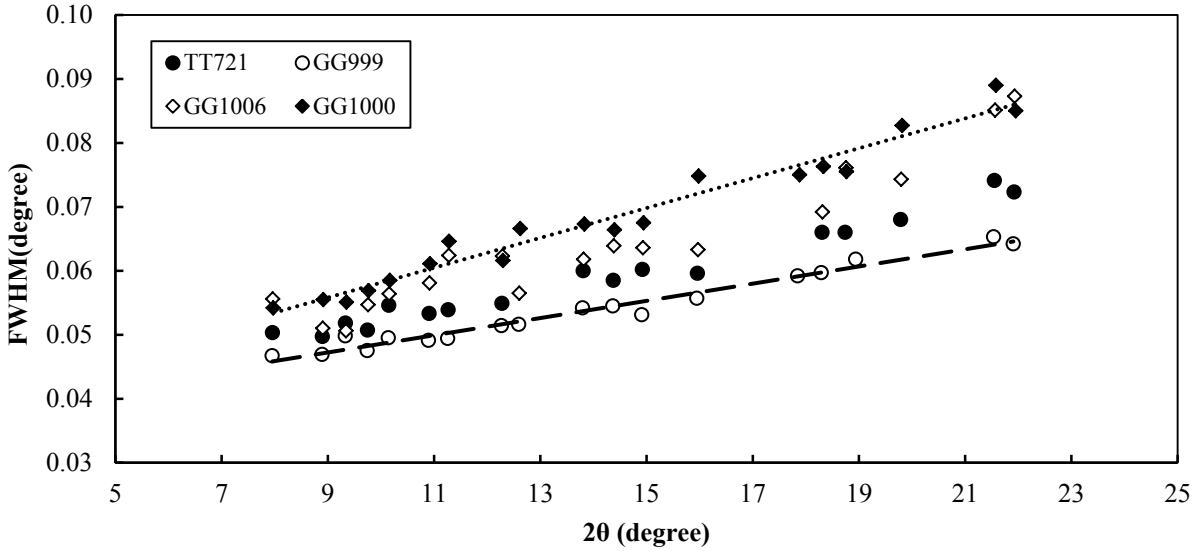

FIGURE 4. XRD peak broadening with diffraction angle 2θ for garnet ($Py_{40}Gr_{60}$). Starting materials for experiments GG999, GG1000, and GG1006 are all same as the product of experiment TT721 synthesized at 1400 ºC. Different annealing paths change the FWHM of XRD peaks. Higher heating temperature (GG1000) caused more XRD peak broadening [dotted line], and longer quenching time to lower temperature (GG999) releases microstrain [dashed line].

669

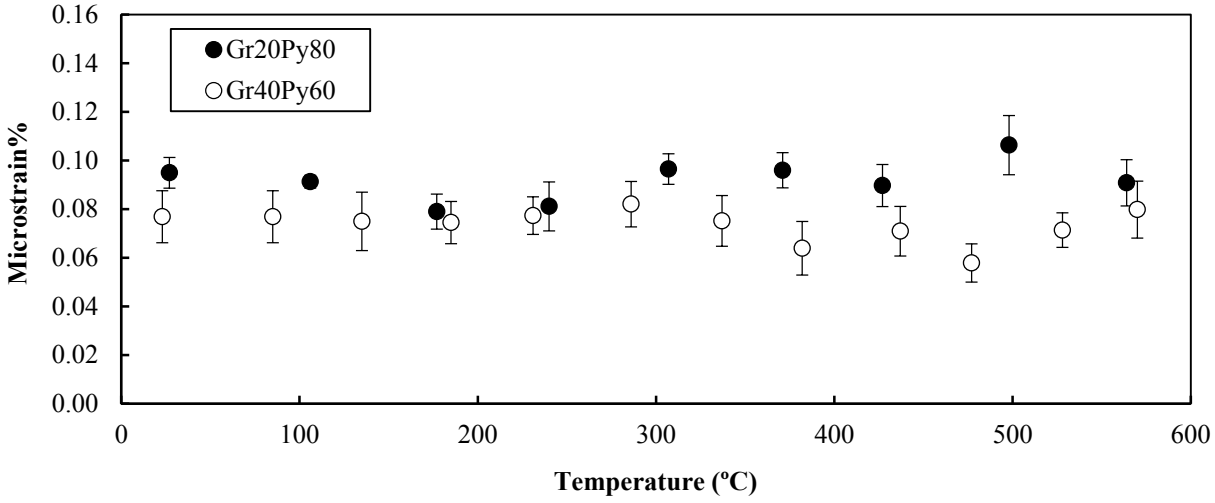

670

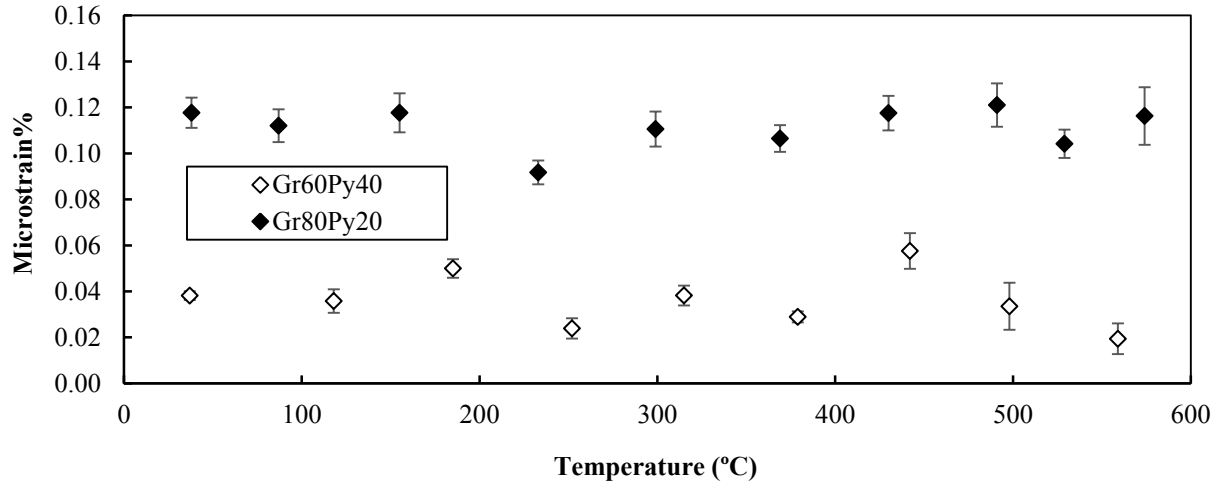

671

672 **FIGURE 5.** Microstrain of garnet solid solutions calculated from Williamson-Hall plot on XRD
673 peak widening data at different temperatures and room pressure. As temperature increased up to
674 600 ºC, there is no systematic variation in microstrain for each garnet solid solution.
675

676

677

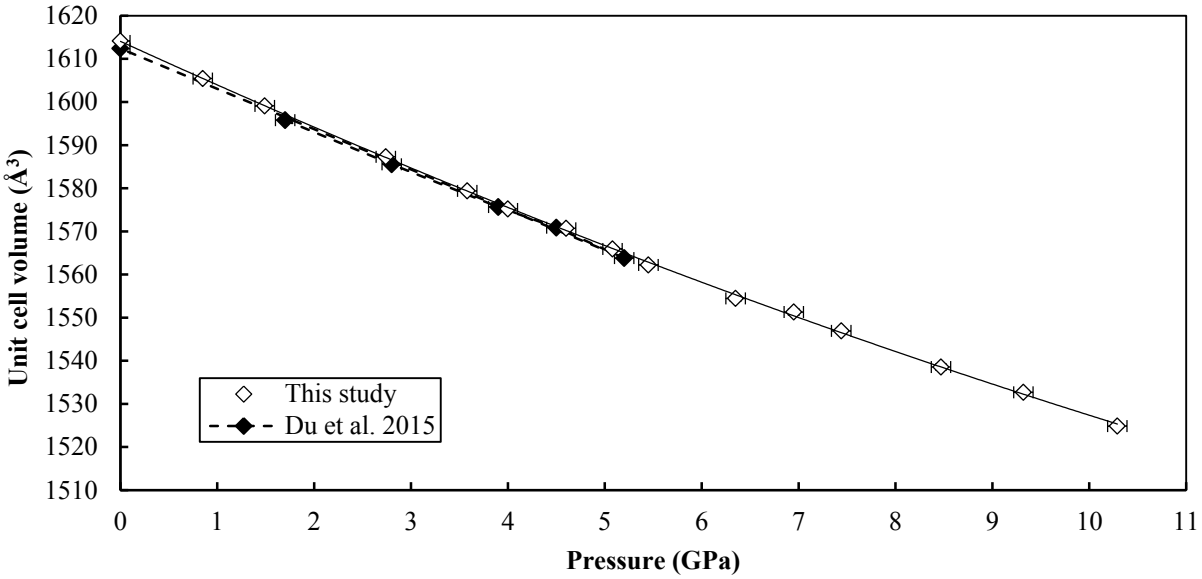

678

679 **FIGURE 6.** Volume compression of garnet with composition $Py_{40}Gr_{60}$ from experiment GG999
680 at high pressure and room temperature. The error bars on the unit cell volume data are smaller
681 than the symbols. The data from Du et al. (2015) were collected at ALS on garnet $Py_{40}Gr_{60}$
682 (TT721)

683

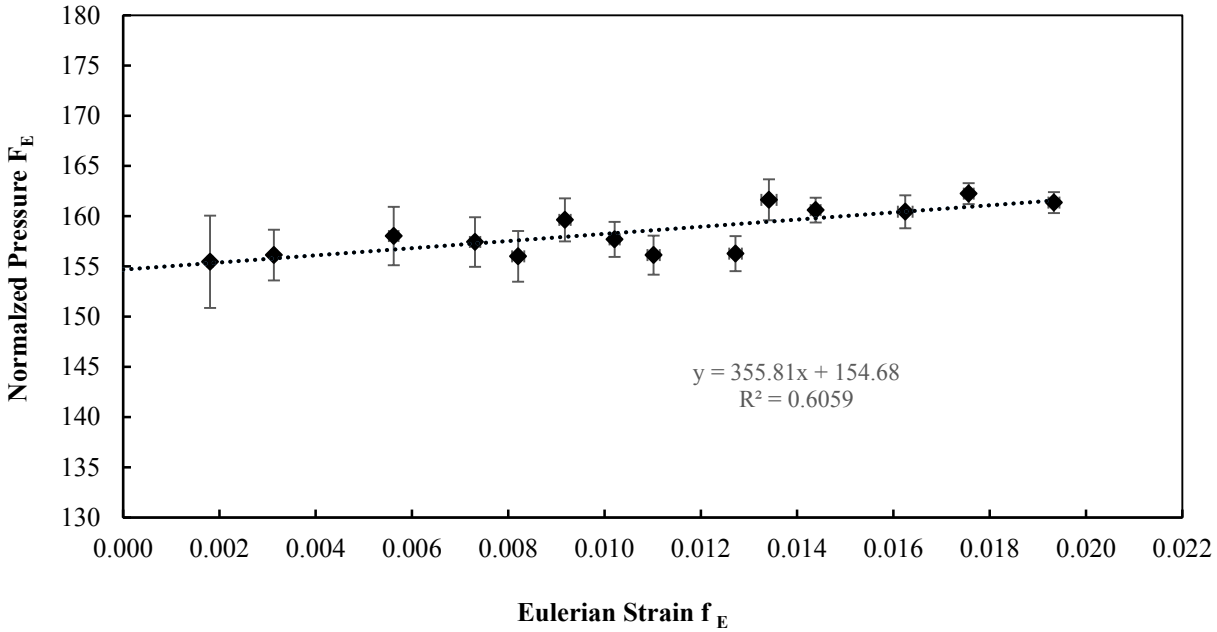

684

685 **FIGURE 7.** Volume Eulerian strain-normalized pressure (F_E-f_E) plot of garnet ($Py_{40}Gr_{60}$) from
686 experiment GG999. The dashed line represents the linear fit through the data.

687

688

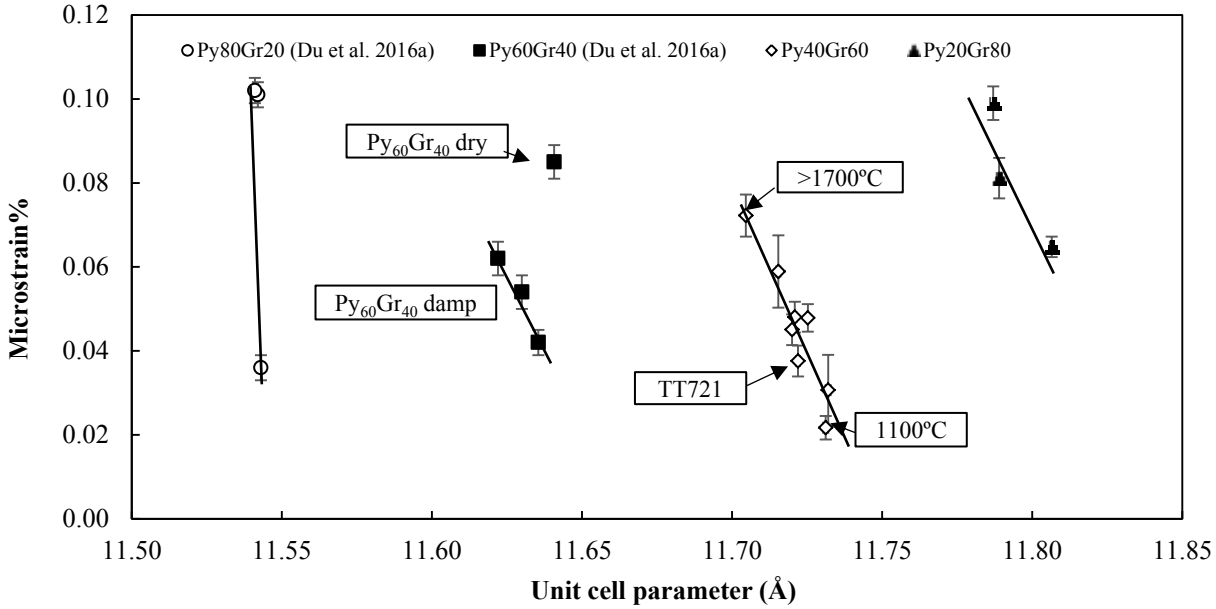

689

690 **FIGURE 8.** Anticorrelation between microstrain and unit cell parameters for garnets synthesized
691 from glass at 6 GPa but annealed at different temperatures for different times given in Tables 1
692 and 2, and from Du et al. (2016). The larger microstrains gained at higher temperature also
693 correspond to a relatively smaller unit cell parameter. The anticorrelation of cell size and
694 microstrain systematically becomes more subdued as the garnets become more pyrope-rich. The
695 offset between the damp and dry $Py_{60}Gr_{40}$ experiments suggests that trace moisture decreases
696 cell size in addition to the effects of the Mg-Ca ordering anticorrelation that is preserved in the
697 damp samples.

698

699

700

701

702

This is a preprint, the final version is subject to change, of the American Mineralogist (MSA)
Cite as Authors (Year) Title. American Mineralogist, in press.
(DOI will not work until issue is live.) DOI: http://dx.doi.org/10.2138/am-2017-6117

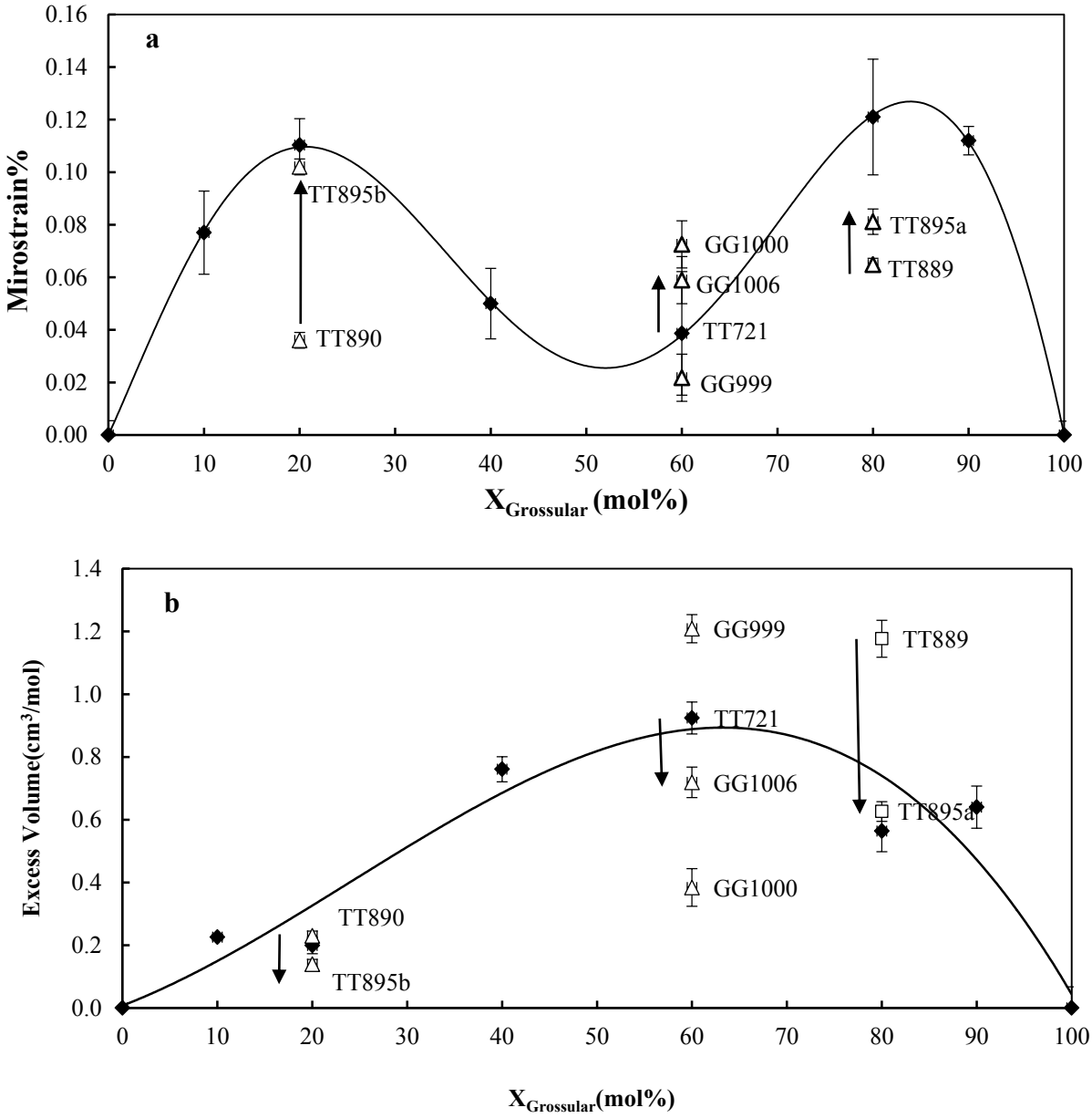

FIGURE 9. a. Microstrain inside garnet structure calculated from X-ray diffraction peak broadening. The solid symbols were reported by Du et al. (2016, 2017) and the open symbols are data from this study presented in Table 1 and Table 2. The arrows indicate the effect of longer annealing time or higher temperature on microstrain. The corresponding changes in unit cell volume are shown in figure **9b**. The relatively smaller changes in microstrain cause large changes on unit cell excess volume for garnets with grossular-rich compositon ($Py_{40}Gr_{60}$ and $Py_{20}Gr_{80}$), but the large changes in microstrain do not change the unit cell volume much for pyrope-rich garnet ($Py_{80}Gr_{20}$) reported by Du et al. (2016). The polynomial fitting curves to the BNL strain and excess volume data emphasize that 1400 °C, 6 GPa, dry garnets have two peaks in strain and one peak in excess volume.

716

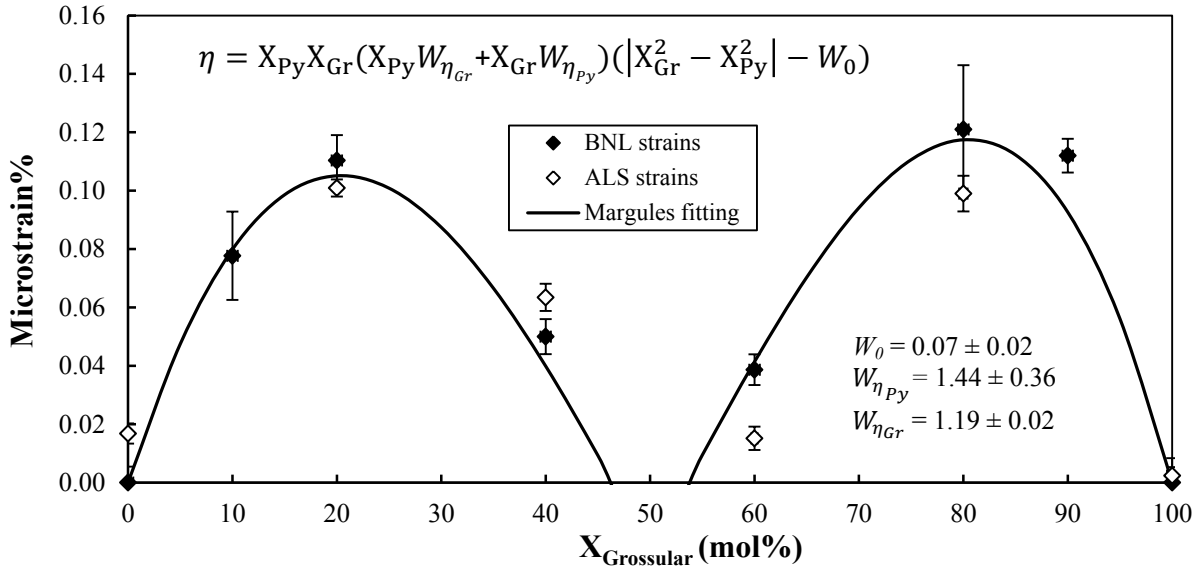

717

718 **FIGURE 10.** Microstrain data from ALS and BNL for dry garnets compared to a Margules-
719 inspired fitting equation. The equation gives a two-peaked distribution of microstrains such as
720 we observe across two independent data collection exercises at two different synchrotrons (ALS
721 and BNL) with acceptable reproducibility. Uncertainties of the fitting parameters were difference
722 calculated from fitting same equation to the two data sets collected at ALS and BNL. The small
723 positive W_o pushes the fitting curve below the horizon of physical reality in a narrow region near
724 equimolar Ca-Mg compositions. This region reflects the disruption in background Mg-Mg or Ca-
725 Ca lattice structure by the intrusion of too many Ca-Mg pairs to allow a recognizable Mg-Mg or
726 Ca-Ca lattice against which to introduce microstrains; i.e. the rationale locally fails.

727